JOURNAL OF MATERIALS SCIENCE 15 (1980) 61–66

Ceramic eutectics in the systems ZrO_2–Ln_2O_3 (Ln = Lanthanide): unidirectional solidification, microstructural and crystallographic characterization

D. MICHEL, Y. ROUAUX, M. PEREZ Y JORBA
L.A. 302, Laboratoire de Chimie Appliquée de l'Etat Solide 15, rue G. Urbain 94400 Vitry, France

Unidirectionally solidified refractory eutectics (melting point between 2100 and 2300° C) in the systems ZrO_2–Ln_2O_3 (Ln = Nd, Sm, Dy) were prepared by "skull-melting". Depending on the growth conditions, different eutectic microstructures were obtained and studied. In particular, well-aligned lamellar eutectics with a great regularity (interlamellar spacing about 10 μm) were observed with sufficiently slow solidification rates (e.g. 0.4 cm h^{-1}). Preferred crystallographic directions for the eutectic growth and epitaxial relationships between phases were determined by X-ray diffraction. Microhardness measurements showed significant reinforcement for eutectics with regard to the pure lanthanide oxide hardness.

1. Introduction

Aligned eutectics have received considerable interest in recent years because of unusual properties resulting from their anisotropic and composite nature [1]. Different ceramic or ceramic–metal eutectics involving refractory oxides such as zirconia or alumina were investigated to prepare materials with high melting point and high strength [2–9].

Poor mechanical properties are exhibited by lanthanide sesquioxides and especially by oxides of the first lanthanide elements (from lanthanum to gadolinium) because of the lamellar character of their structure. Moreover their sensitivity to hydration and carbonization in air produces a rapid decohesion of bulk materials.

In order to obtain materials based on Ln_2O_3 presenting a better mechanical and chemical behaviour with regard to liquid or gaseous corrosion, composites were prepared in the systems ZrO_2–Ln_2O_3. Samples with a regular distribution of two phases were obtained after solidification of ternary oxide eutectics. When the freezing run was achieved in a sufficient temperature gradient, directional microstructures consisting of parallel fibres or lamellae were formed.

In the eutectics considered, a "stabilized" zirconia phase (with a fluorite-type oxygen-deficient structure) is associated with the lanthanide oxide phase. Three different crystallographic forms are displayed by lanthanide sesquioxides at room temperature: trigonal (A-type), monoclinic (B-type), cubic (C-type). Eutectics involving Nd_2O_3, Sm_2O_3 and Dy_2O_3 with, respectively, an A, B and C structure were especially prepared at the compositions given by the high-temperature phase diagrams established by Rouanet [10].

2. Experimental details

2.1. Preparation of aligned eutectics

Mixtures with eutectic composition of Ln_2O_3 (Rhone-Progil 99.9% pure) and dehafnied ZrO_2 (Ugine 99.9% pure) powders were melted by direct coupling of high-frequency currents (4 to 6 MHz) provided by a 20 kW Toccostel generator. The melt (about 300 g molten material) was contained in a copper-cooled crucible (5 cm i. d., 6 cm high) within a crust of its own powder

0022–2461/80/010061–06$02.60/0 © *1980 Chapman and Hall Ltd.*

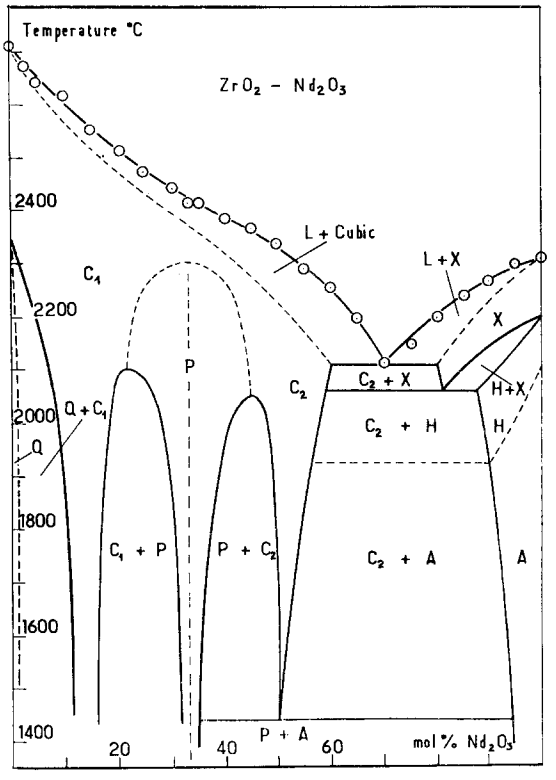

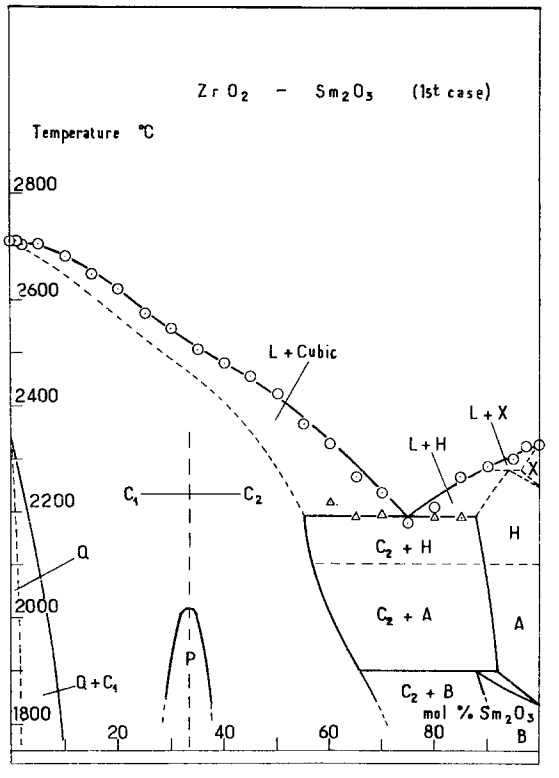

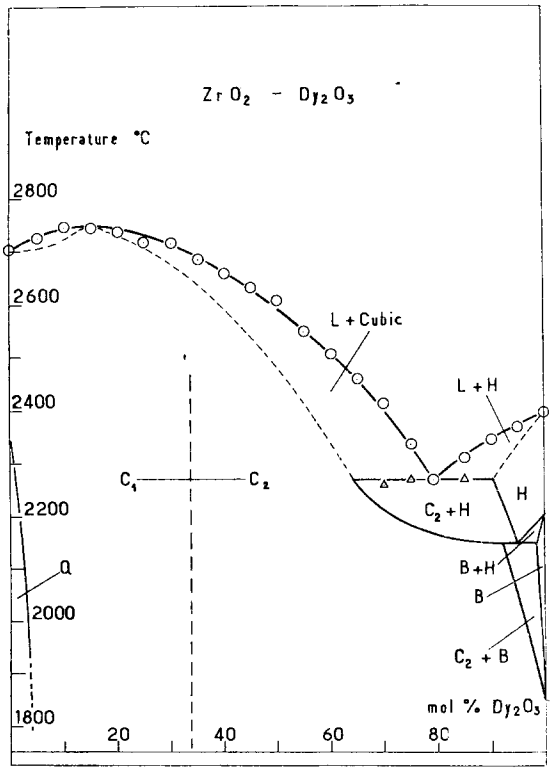

Figure 1 High-temperature phase diagrams of ZrO_2–Ln_2O_3 after Rouanet [10].

according to the so-called "skull melting" technique [11, 12].

Solidification results from a controlled decrease of the output power. The freezing front progresses across the ingot from the lateral walls and the bottom sole. In the central zone, the solid–liquid interface moves perpendicular to the axis of the cylindrical crucible.

Various cooling programmes allow eutectic growth rates, R, in the internal zone with $0.04 < R < 4$ cm h^{-1}. In this study, experiments were performed at two different rates, $R = 0.4$ and 2 cm h^{-1}.

2.2. Characterization of the eutectics

Sections perpendicular and parallel to the growth axis were cut off, and polished surfaces were examined by optical microscopy after etching by hot concentrated sulphuric acid.

Eutectic phases were identified by X-ray diffraction and their chemical composition determined from values of unit-cell parameters which vary appreciably with the zirconium oxide content. Local analysis of samples were carried out using an electron microprobe from the intensity of $L\alpha$ X-lines of zirconium and lanthanides.

X-ray "rotating crystal" patterns of needles cut off parallel to the solidification direction gave

the preferred crystallographic growth axes. Epitaxial relationships between eutectic phases were established from de Jong–Bouman patterns.

3. Results

3.1. Structure and composition of the eutectic phases

All the systems ZrO_2–Ln_2O_3 (Ln = lanthanide) present a eutectic with a high rare-earth content. The eutectic composition varies from 62 mol% for La_2O_3 to 82 mol% for Yb_2O_3 [10]. For the oxides considered, the eutectic compositions are, respectively, 70 mol% Nd_2O_3–30 mol% ZrO_2, 75 mol% Sm_2O_3–25 mol% ZrO_2, and 79 mol% Dy_2O_3–21 mol% ZrO_2 as shown in Fig. 1.

One eutectic phase is a solid solution of zirconia in the lanthanide oxide, its structure is trigonal (A-type) for Nd_2O_3, monoclinic (B-type) for Sm_2O_3, and cubic (C-type bixbyite) for Dy_2O_3. The second phase with the formula $Zr_{1-x}Ln_xO_{2-x/2}$ ($0.6 < x < 0.8$ for Ln = Nd → Dy) possesses a fluorite structure with oxygen vacancies ($x/2$ for two oxygen ions).

3.1.1. Eutectic Nd_2O_3 70 mol%–ZrO_2

Two phases were found: trigonal A, $a = 3.806$ Å, $c = 5.983$ Å; cubic (fluorite-type), $a = 5.421$ Å. These parameters correspond, respectively, to phases with 89 mol% Nd_2O_3 and 56 mol% Nd_2O_3.

3.1.2. Eutectic Sm_2O_3 75 mol%–ZrO_2

Three phases were detected: a monoclinic B-type phase, $a = 14.05$ Å, $b = 3.615$ Å, $c = 8.782$ Å, $\beta = 100°4$, with composition estimated to be 91 mol% Sm_2O_3; two cubic fluorite-type phases with parameters, $a_1 = 5.347$ Å (Sm_2O_3 52 mol%), $a_2 = 5.385$ Å (Sm_2O_3 64 mol%).

From Debye–Scherrer line intensities, the volume of the phase richer in zirconia (Sm_2O_3 52 mol%) amounts to about four times the other (Sm_2O_3 64 mol%). The phase diagram shows that this major phase corresponds to the cubic phase solidified at 2200° C together with the primary high-temperature hexagonal (H) phase.

The second cubic phase (64 mol% Sm_2O_3) and the monoclinic phase result from the peritectoid decomposition of the A phase at 1900° C.

3.1.3. Eutectic Dy_2O_3 79 mol%–ZrO_2

Two cubic phases (bixbyite-type) are present with parameters $a_1 = 10.605$ Å (composition 73 mol% Dy_2O_3), $a_2 = 10.627$ Å (composition 84 mol% Dy_2O_3).

3.2. Crystallographic relationships

The preferred crystallographic directions for the eutectic growth are $\langle 1\,1\,0\rangle$ for cubic phases (with fluorite or bixbyite-type structures) $\langle 0\,1\,\bar{1}\,0\rangle$ for the trigonal A-type phase, $\langle 1\,\bar{3}\,2\rangle$ for the B-type monoclinic phase.

The two eutectic phases are related by the following conditions of epitaxy:

(a) trigonal A – fluorite F $(0\,0\,0\,1)_A \parallel (1\,1\,1)_c$
(Nd_2O_3) $[0\,\bar{1}\,1\,0]_A \parallel [1\,\bar{1}\,0]_c$

(b) monoclinic B – fluorite F $(2\,0\,\bar{1})_B \parallel (1\,1\,1)_c$
(Sm_2O_3) $[1\,\bar{3}\,2]_B \parallel [1\,\bar{1}\,0]_c$

(c) syntaxy for two cubic phases (Dy_2O_3).

In the Nd_2O_3–ZrO_2 eutectic, the $(1\,1\,1)_C$ and $(0\,0\,0\,1)_A$ planes present the same hexagonal symmetry and close interatomic distances, respectively, 3.833 and 3.806 Å. Therefore, epitaxy requirements for the symmetries and the lattice match at the interface are satisfied.

For the Sm_2O_3–ZrO_2 eutectic, the same relation appears between the cubic and monoclinic phase by considering the monoclinic phase as a distorted arrangement of the trigonal A-type. The $(2\,0\,\bar{1})_B$ plane is homologue of the $(0\,0\,0\,1)_A$ plane and presents a pseudo-hexagonal symmetry. The angles between the $[1\,\bar{3}\,2]$, $[1\,3\,2]$, $[0\,1\,0]$ directions corresponding to $\langle 1\,0\,\bar{1}\,0\rangle$ trigonal axes are respectively 118°, 118° and 124°. Atomic distances in this $(2\,0\,\bar{1})_B$ plane are 3.856 and 3.615 Å. For the cubic phases met in the Sm_2O_3–ZrO_2 eutectic, atomic separations in the $(1\,1\,1)$ plane are 3.781 Å for the primary eutectic phase (Sm_2O_3 52 mol%) and 3.808 Å for the secondary eutectoid phase (Sm_2O_3 64 mol%).

3.3. Microstructure

The general aspect of the eutectics is lamellar with a fairly regular interlamellar spacing λ about 10 μm.

Figs. 2 and 3 show longitudinal and transverse sections of the Nd_2O_3–ZrO_2 eutectic grown at $R = 0.4$ cm h^{-1} with an interlamellar spacing $\lambda = 14$ μm and of the Dy_2O_3–ZrO_2 eutectic $R = 2$ cm h^{-1} and $\lambda = 9$ μm.

Samples grown with the lower solidification rate (0.4 cm h^{-1}) present a more regular arrangement and a larger interlamellar spacing than those with $R = 2$ cm h^{-1}. In the limited range of R investigated, the relation $\lambda^2 R$ = constant proposed

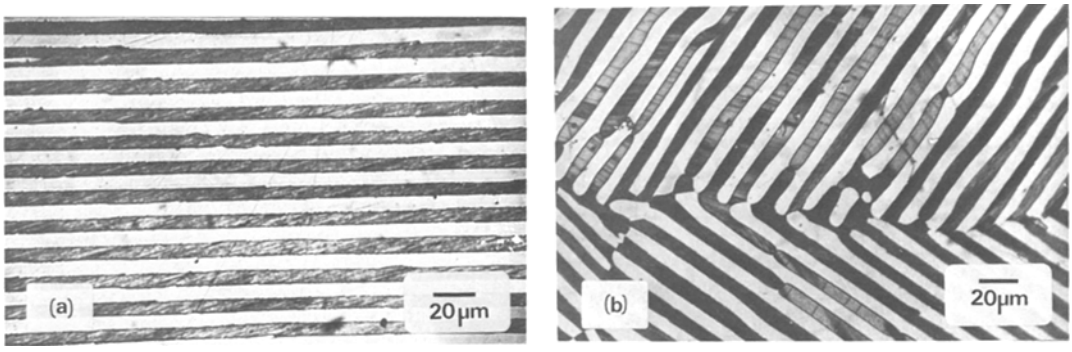

Figure 2 Eutectic Nd_2O_3–ZrO_2, $R = 0.4$ cm h^{-1}. (a) Longitudinal section, (b) transverse section.

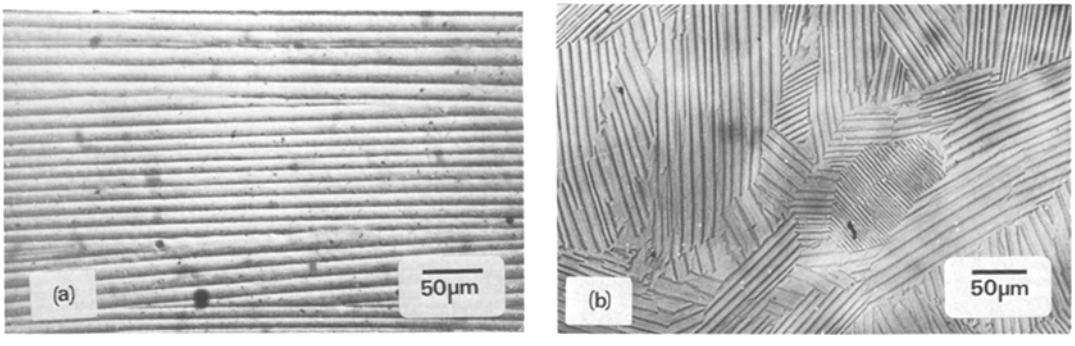

Figure 3 Eutectic Dy_2O_3–ZrO_2, $R = 2$ cm h^{-1}. (a) Longitudinal section, (b) transverse section.

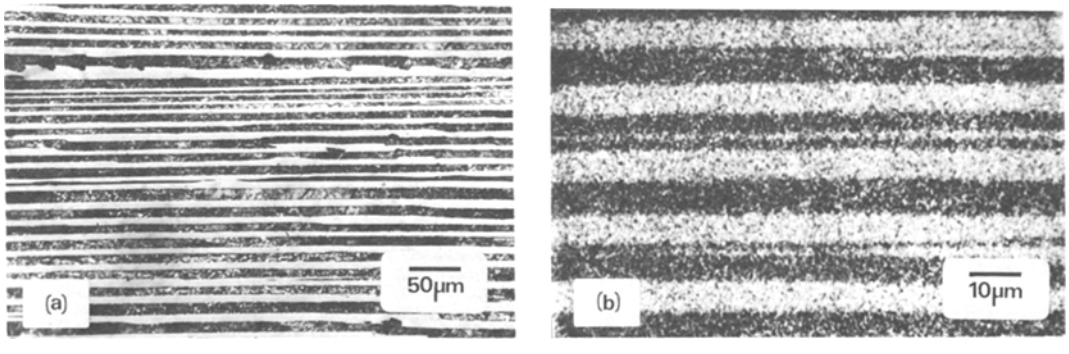

Figure 4 Eutectic Sm_2O_3–ZrO_2, $R = 0.4$ cm h^{-1}. Longitudinal section (a) optical microscopy observation, (b) electron microprobe image, obtained with the $L\alpha$ line of zirconium.

by Tiller [13] and developed by Hunt and Jackson [14, 15] and followed by most ceramic eutectics [3, 4, 6] is obeyed. For instance, the values $\lambda = 15\ \mu m$ (Fig. 4) for $R = 0.4$ cm h^{-1} and $\lambda = 7\ \mu m$ for $R = 2$ cm h^{-1} obtained in the Sm_2O_3–ZrO_2 eutectics lead to $\lambda^2 R \simeq 0.9\ 10^{-6}$ $cm^3\ h^{-1}$. Similar constants are obtained for the Nd_2O_3 and Dy_2O_3 eutectics and are comparable with the values $\lambda^2 R = 2.38\ \ 10^{-6}$ $cm^3\ h^{-1}$ for the ZrO_2–Y_2O_3 eutectic [4] and $\lambda^2 R = 0.2\ 10^{-6}\ cm^3\ h^{-1}$ for the ZrO_2–MgO eutectic [6].

For the Nd_2O_3 and Sm_2O_3 eutectics, a regular alternation of dark and light lamellae was observed. The darker zones were identified as the phase richer in lanthanide by electron microprobe analysis as seen in Fig. 4b. These zones with either an A or B-type structure are more readily etched and present a lower microhardness than regions of the fluorite phase.

With high magnification, a fine microstructure is visible inside dark lamellae, as for instance in the Sm_2O_3 eutectic shown in Fig. 5. This secondary

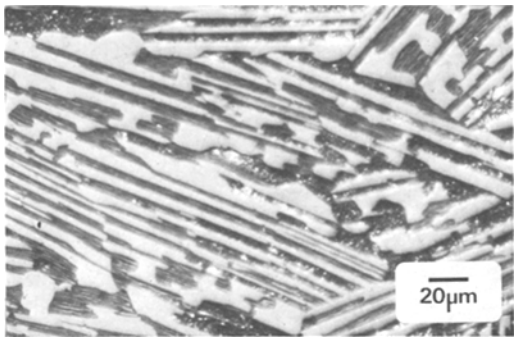

Figure 5 Eutectic Sm_2O_3–ZrO_2, $R = 2$ cm h^{-1}. Transverse section, the eutectoid decomposition is visible in dark lamellae.

controlled, a dendritic growth is observed. Fig. 7 shows typical examples of columnar and fibrous dendritic structures. Such structures are successively obtained with increasing G/R values, composite structures such as in Figs. 2 to 6 are only observed with a sufficiently high G/R ratio [16, 17].

3.4. Microhardness

Microhardness tests were performed with a Vickers indenter with various charges ranging between 50 and 200 g. The size of indents (from 5 to 25 μm) allow the hardness measurement for each eutectic phase and for the global eutectic.

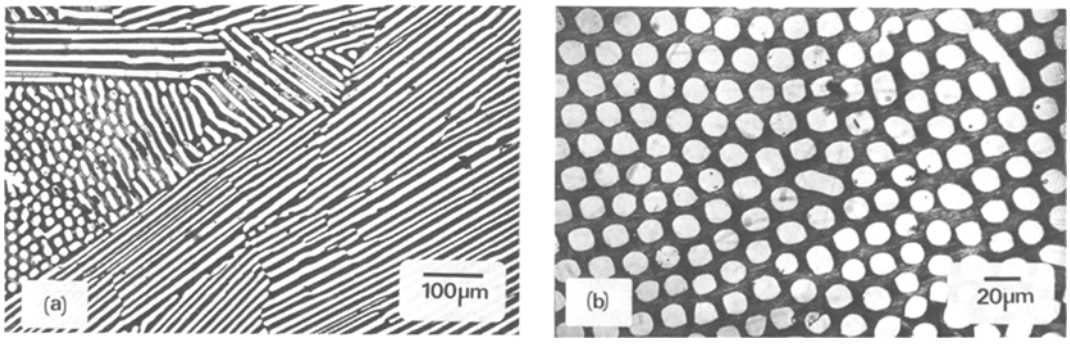

Figure 6 Eutectic Nd_2O_3–ZrO_2, $R = 0.4$ cm h^{-1}. Transverse section showing (a) both fibrous and lamellar structures, (b) fibres of the cubic phase.

structure is attributed to the eutectoid decomposition into a second cubic phase and either the trigonal (for Nd_2O_3) or the monoclinic (for Sm_2O_3) phase. X-ray diffraction results indicate this for Sm_2O_3 by the presence of small amounts of a second fluorite-type phase.

Because of the small scale (less than 1 μm) of this phenomenon, the microprobe resolution did not allow distinction of the two phases within the primary dark lamellae.

In addition to the general lamellar structure, small sized domains with a fibrous microstructure are sometimes observed among the lamellar eutectic. An example is given in Fig. 6 for an Nd_2O_3–ZrO_2 eutectic.

All the previously described composite eutectics were obtained in the internal part of the ingot where solidification progresses with a plane-front. In contrast with these well-aligned microstructures, a variety of non-plane front structures are found in the outer parts of ingots. In these regions (near the cooled crucible) where the temperature gradient G and the solidification rate R are un-

As appears from Table I, the hardness is markly higher for eutectics than for pure lanthanide oxides. An appreciable reinforcement is also produced by the addition of zirconia to the lanthanide oxide phase.

For neodymium oxide eutectics, the measured hardness 550 kg mm^{-2} in the fibrous microstructure (e.g. in Fig. 6b) is lower than that for the lamellar eutectic (720 kg mm^{-2}).

The difference in hardness between transverse and longitudinal sections were not significant.

4. Conclusions

Plane-front growth occurs in the ZrO_2–Ln_2O_3 eutectics (Ln = Nd, Sm, Dy) at solidification rates $R = 0.4$ and 2 cm h^{-1}. Aligned lamellar eutectics with an interlamellar spacing about 10 μm are formed. The observed epitaxial relationships have established that the eutectic phases share dense planes with hexagonal (or nearly so) symmetry. Preliminary studies have shown appreciable improvements of mechanical properties and of resistance to hydration.

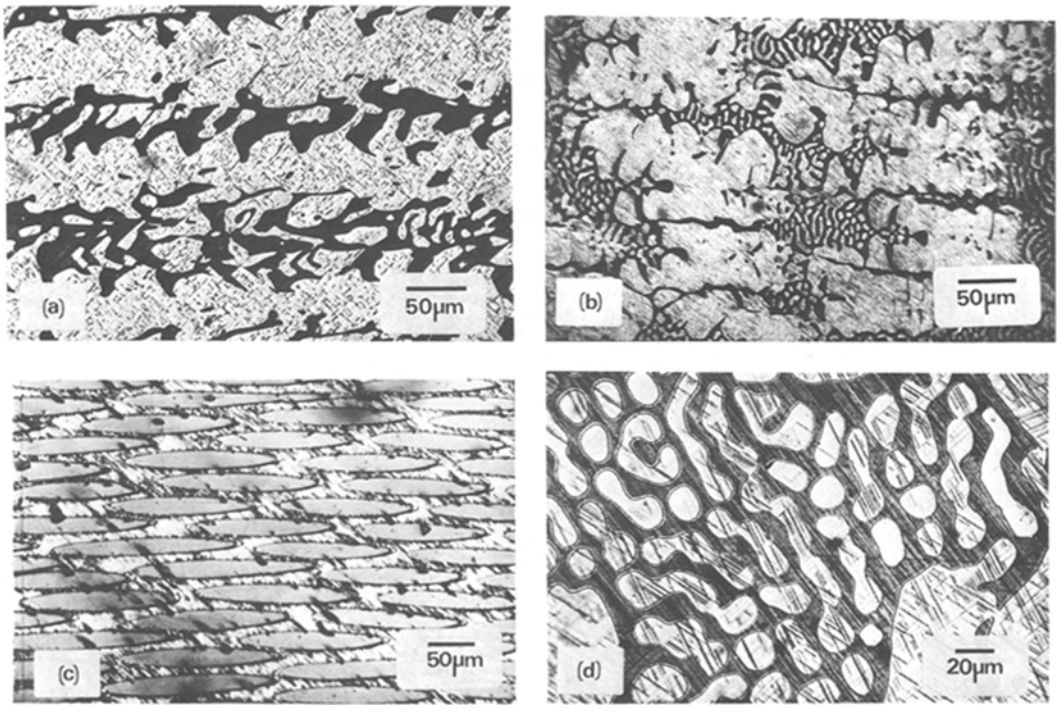

Figure 7 Eutectic $Nd_2O_3-ZrO_2$. Dendritic growth observed in outer parts of the ingot. Dendritic columns: longitudinal (a) and transverse (b) sections. Fibrous dendrites: longitudinal (c) and transverse (d) sections.

TABLE I Vickers microhardness (kg mm^{-2}) of the eutectic phases $ZrO_2-Ln_2O_3$ compared with values measured on Ln_2O_3 crystals [18]

Lanthanide	Cubic phase	Global eutectic	Lanthanide oxide eutectic phase	Pure lanthanide sesquioxide
Nd	1100	720	500	380
Sm	1000	770	680	415
Gd	1100	1000	800	750

Acknowledgement

The authors thank C. Bahezre (C.N.R.S. Bellevue) for the electron microprobe measurements.

References

1. W. ALBERS, in "Preparative methods in solid state chemistry" edited by P. Hagenmuller (Academic Press, New York, 1972) pp. 367–99.
2. F. SCHMID and D. VIECHNICKI, *J. Mater. Sci.* 5 (1970) 470.
3. F. L. KENNARD, R. C. BRADT and V. S. STUBICAN, *J. Amer. Ceram. Soc.* 56 (1973) 566.
4. C. O. HULSE and J. A. BATT, Conference on In-Situ Composites Technical Report NMAB 308, Vol. 1 (1973) pp. 129–40.
5. M. D. WATSON, T. A. JOHNSON, J. F. BENZEL and A. T. CHAPMAN, *ibid* pp. 157–68.
6. F. L. KENNARD, R. C. BRADT and V. S. STUBICAN, *J. Amer. Ceram. Soc.* 57 (1974) 428.
7. J. W. STENDERA and J. F. BENZEL, *ibid* 58 (1958) 116.
8. N. CLAUSSEN and K. RÖSER, *Mat. Res. Bull.* 12 (1977) 393.
9. R. L. ASHBROOK, *J. Amer. Ceram. Soc.* 60 (1977) 428.
10. A. ROUANET, *Rev. Int. Hautes Temper. Refract.* 8 (1971) 161.
11. D. MICHEL, *ibid* 9 (1972) 225.
12. D. MICHEL, M. PEREZ Y JORBA and R. COLLONGUES, *J. Crystal Growth* 43 (1978) 546.
13. W. A. TILLER, in "Liquid metals and solidification" (ASM, Cleveland, Ohio, 1958) pp. 276–318.
14. J. D. HUNT and K. A. JACKSON, *Trans. Met. Soc. AIME* 236 (1966) 843.
15. K. A. JACKSON and J. D. HUNT, *ibid.* 236 (1966) 1129.
16. M. C. FLEMINGS, in "Surfaces and Interfaces", Vol. II (Syracuse University Press, New York, 1968) pp. 313–51.
17. J. W. RUTTER, *J. Crystal Growth* 42 (1977) 515.
18. A. M. LEJUS, *Rev. Int. Hautes Temp. Réfract.* 13 (1976) 89.

Received 24 May and accepted 28 June 1979.